# Unimolecular Dissociation of Formyl Radical, HCO → H + CO, Studied over 1−100 Bar Pressure Range

**Lev N. Krasnoperov* and Evgeni N. Chesnokov†**

*Department of Chemistry and Environmental Science, New Jersey Institute of Technology, University Heights, Newark, New Jersey 07102*

**Harald Stark and A. R. Ravishankara‡**

*NOAA, Aeronomy Laboratory, R/AL2, 325 Broadway, Boulder, Colorado 80305-3328, and the Cooperative Institute for Research in Environmental Sciences, University of Colorado, Boulder, Colorado 80309-0216*

*Received: May 31, 2004; In Final Form: September 23, 2004*

Unimolecular dissociation of formyl radical, HCO → H + CO (1), was studied using pulsed laser photolysis coupled to transient UV−vis absorption spectroscopy. One-pass UV absorption, multipass UV absorption, and cavity ring down spectroscopy in the red spectral region were used to monitor temporal profiles of the HCO radical. A heatable high-pressure flow reactor of a new design was employed. Reaction 1 was studied over a buffer gas (He) pressure range 0.8−100 bar and a temperature range 498−769 K. Formyl radicals were prepared by pulsed photolysis of acetaldehyde and propionaldehyde (308 nm, XeCl excimer laser, 320 nm, doubled dye laser). In addition to formyl radicals monitored at 230 and 613.8 nm, methyl radicals were monitored via absorption at 216.5 nm. The initial concentrations of free radicals were varied between $7 \times 10^{10}$ and $8 \times 10^{13}$ molecules cm$^{-3}$. The obtained second-order rate constant at 1 bar is $k_1(\mathrm{He}) = (0.8 \pm 0.4) \times 10^{-10} \exp(-66.0 \pm 3.4 \text{ kJ mol}^{-1}/RT)$ cm$^3$ molecule$^{-1}$ s$^{-1}$ (498−769 K). The low-pressure data of this study were combined with those from a high-temperature shock tube study and the low-temperature data on the reverse reaction to yield $k_1(\mathrm{He}) = (0.60 \pm 0.14) \times 10^{-10} \exp(-64.2 \pm 1.4 \text{ kJ mol}^{-1}/RT)$ cm$^3$ molecule$^{-1}$ s$^{-1}$ over an extended temperature range, 298−1229 K. The dissociation rate constants measured in this work are lower than previously reported by a factor of 2.2 at the highest temperature of our measurements and a factor of 3.5 at the low end. Our experimental data indicate a pressure dependence of the second-order rate constant for the dissociation of formyl radical (1), which is attributed to pressure falloff expected from the theory of isolated resonances.

## Introduction

Reaction of unimolecular dissociation of formyl radical (HCO) is of considerable importance in the hydrocarbon combustion mechanisms:[1−5]

$$\mathrm{HCO} \rightarrow \mathrm{H} + \mathrm{CO} \qquad (1)$$

The methyl radical, produced in H-atom abstraction reactions from methane is converted to formaldehyde in reaction with oxygen atoms. The formyl radical is produced by H-atom abstraction from formaldehyde. Subsequently, unimolecular decomposition of formyl radical (reaction 1) leads to chain branching via interaction of hydrogen atoms with molecular oxygen. Competition between the unimolecular dissociation of formyl radical (reaction 1) with reactions of HCO with $O_2$, OH, and H controls the chain branching rate and, therefore, a number of important characteristics of combustion (such as the thresholds for and delays in autoignition, the flame propagation speed, etc.).[1−5]

Formyl radical also received significant attention in recent years due to its "non-classical RRKM" behavior. The radical has a relatively weak C−H bond (bond energy is 63.2 kJ mol$^{-1}$ [6] and large vibrational frequencies. As a result, the radical has isolated resonances at energies above the dissociation threshold. These resonances have been extensively studied using both spectroscopy and theory.[7−13] This feature is expected to have a significant impact on the kinetics of reaction 1, particularly on the pressure falloff curve.[14] Because of the isolated resonances the high-pressure rate constant for the reverse reaction (H + CO addition) is about 2.5 orders of magnitude lower than that expected for a "regular" RRKM behavior.[14] The long lifetime of the resonances (compared to the lifetime of a collision complex that obeys classical RRKM behavior) is expected to lower the characteristic transition pressure from about 3000 bar to ca. 10 bar around 300 K.[14]

Despite the importance of this reaction in combustion mechanisms and for the fundamental chemical kinetics, there were only a few direct studies of reaction 1 under the conditions of thermal activation until recently.[15] Most previous information on the kinetics of this reaction was obtained either from complex reaction mechanisms (such as formaldehyde[16] and acetylene[17] flames, photooxidation of acetone,[18] and pyrolysis of formaldehyde[19]) or from the kinetics of the reverse reaction[20−27] using the reaction thermochemistry. The first direct study of reaction

* To whom correspondence should be addressed. Fax: 973-596-3586. E-mail: krasnoperov@adm.njit.edu.

† Permanent address: Institute of Chemical Kinetics and Combustion, Siberian Branch of Russian Academy of Sciences, Novosibirsk 630090, Russia.

‡ Also affiliated with the Department of Chemistry and Biochemistry, University of Colorado, Boulder, CO 80309.

10.1021/jp0403994 CCC: $27.50 
Published on Web 12/08/2004

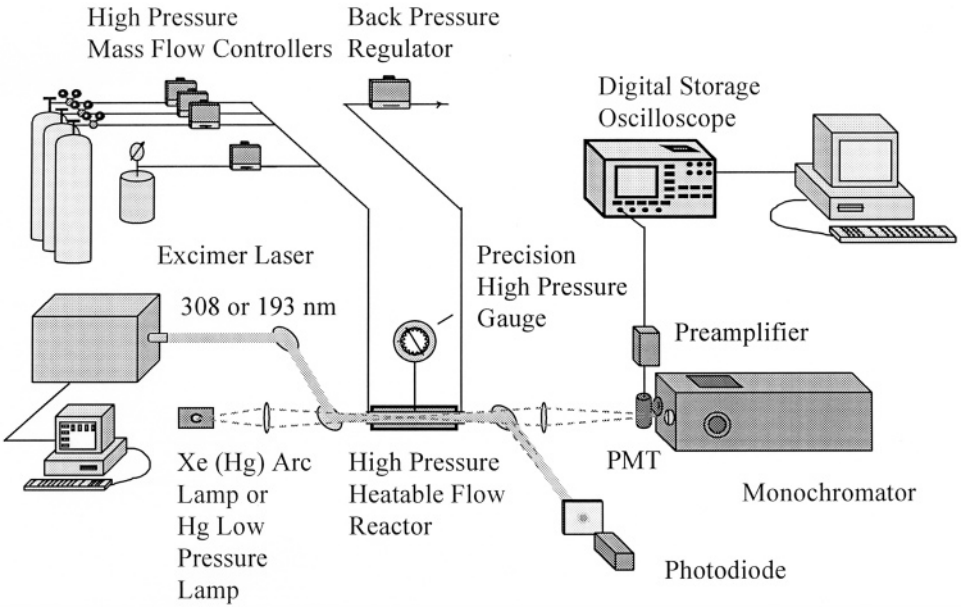


**Figure 1.** Experimental setup used for studying the kinetics of the thermal decomposition of HCO by monitoring HCO via absorption. Pulsed excimer laser photolysis was used to create HCO, and UV−vis transient absorption spectroscopy was used to monitor HCO in a high-pressure flow system.

1 employed laser photolysis combined with photoionization mass spectrometry.[15] The buffer gas pressure in this work was less than 0.015 bar. At these pressures the reaction is well into the low-pressure region at the temperatures used in this study and information on the transition region and the high-pressure limit rate constant could not be derived.

The current work summarizes direct studies of reaction 1 performed during the last four years using laser pulsed photolysis combined with transient absorption spectroscopy in the visible and UV regions.[28−31] Reaction 1 was directly studied over an extended buffer gas pressure range (1−100 bar) using a variety of experimental techniques. Single-pass and multipass UV absorption[28,30] as well as CRDS detection[32] using the red transition of the HCO radical were employed. The results of these measurements are in considerable discrepancy (factor 2−3) with the previous data.[15] In addition, the second order rate constant of reaction 1 was observed to depend on pressure, which is tentatively attributed to a shift in the pressure falloff due to the "non-RRKM" behavior of HCO radical decomposition.

## Experimental Section

Two experimental facilities were used to study reaction 1. In both cases laser photolysis was used to produce HCO radicals. Transient UV absorption using single-pass and multipass cells was used in the experiments performed at NJIT. Cavity ring down spectroscopy (CRDS) on the red transition of HCO was used to monitor the temporal profiles of the radical in the experiments performed at NOAA.

The experimental facility at NJIT consists of excimer laser photolysis coupled to UV−vis transient absorption spectroscopy and a high-pressure flow system (Figure 1). Some details of the experimental arrangements and the signal accumulation are described elsewhere.[33,34] Helium was used as the buffer gas. The measurements were performed over the 1−100 bar pressure and 282−496 °C temperature ranges. A heatable high-pressure flow reactor of a novel design was employed (Figure 2). The reactor was made of 12.7 mm o.d. ($^1/_2$ in.) stainless steel tubing. The central part of the tube (20 cm) was inserted into an aluminum cylindrical block, which serves as a heat distributor.

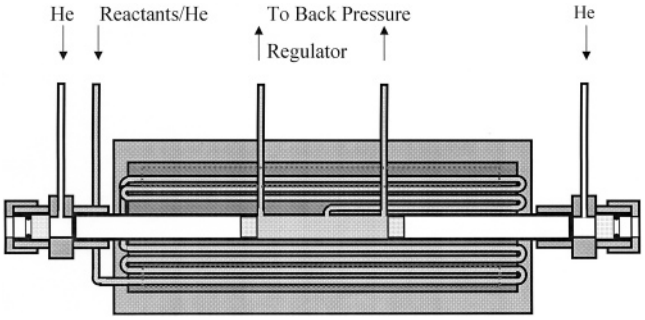


**Figure 2.** Cross-section of the heatable high-pressure flow reactor.

Two electrical resistance heaters were located within the aluminum block parallel to the reactor. A thermocouple (K-type, Omega) was located in the middle of the block. The reagents were supplied through a 3.175 mm o.d. ($^1/_8$ in.) stainless steel tube that was passed seven times (total length 140 cm) through the aluminum block for preheating. Such an arrangement ensured complete preheating of the reactant mixture to the reactor temperature without using additional ovens and temperature controllers. Calculations based on the Graetz formula for gas heating in a Poiseuille's flow[35] show guaranteed preheating of the gas flow well within 0.001 K both for He and $N_2$ for the experimental conditions used in the current work.

Two UV-grade quartz windows (12.7 in diameter, 9.5 mm thick) were sealed at the end of the reactor at ambient temperature outside the high-temperature zone using Viton O-rings. The preheated reactant mixture entered the reactor tube in the center and left through two outlets located on two sides 5 cm away from the center but within the uniform temperature zone. Additional buffer gas flows entered the reactor near the windows to flush gas from the windows toward the outlets. Such an arrangement allowed us to keep the reactants in the uniform temperature zone and avoid having to seal windows at elevated temperatures. This configuration was found to work satisfactorily at low to moderate pressures (1−10 bar). At higher pressures, convection developed at the ends of the reactor due to the large temperature gradients. Convection led to "spreading" of the reactants toward the windows into the cooled zone. In addition,

it led to deflection of the monitoring light beam due to the vertical gradient in the refraction index in the convection zones. To suppress convection, two additional thick (9.5 mm) quartz windows were placed without sealing inside the reactor at the reactor outlets. The optical path in the zone of reactants was 10.0 cm. This "four windows" configuration prevented penetration of the reactants out of the observation zone and suppressed the monitoring beam deflection.

The axial temperature profiles were measured in 1 cm steps along the reactor length for each set of the experimental conditions (the temperature set points, total flows and pressures) used in the kinetic measurements. One of the windows was replaced by a movable coaxial 1.6 mm o.d. K-type thermocouple ($^1/_{16}$ in.) sealed using a commercial adapter. In cases when internal windows were installed, one of these windows was replaced with a ceramic cylinder with a hole in the center for the thermocouple. The temperature profiles were uniform within $\pm 5$ K in the reactant zone. Average temperature in the reactant zone was taken as the reactor temperature.

Formyl radicals were prepared by pulsed photolysis of acetaldehyde and propionaldehyde at 308 nm (XeCl excimer laser):

$$CH_3CHO + h\nu(308\ \text{nm}) \rightarrow CH_3 + HCO \qquad (2a)$$

$$\rightarrow CH_4 + CO \qquad (2b)$$

$$C_2H_5CHO + h\nu(308\ \text{nm}) \rightarrow C_2H_5 + HCO \qquad (3)$$

Photolysis of acetaldehyde at 308 nm occurs primarily via channel 2a.[36−46] Minor channel 2b produces methane and carbon monoxide, which do not lead to any kinetic interference under the experimental conditions of the current study.

The kinetics of formyl radical decay was monitored by absorption in the UV (at 230 and 254 nm),[47] as well as in the visible at 614.6 nm (with fwhm = 1.0 nm). Two experimental arrangements were used: a one-pass cell and a multipass cell.

**One-Pass Experiments.** The output from a Xe arc lamp (75 W, Oriel Instruments) was focused into the cell and then onto the entrance slit of a monochomator using two fused silica lenses. Low initial HCO concentrations ($(3.2-78) \times 10^{12}$ molecules $cm^{-3}$ with absorptions in the range 0.023−0.57%) were used to minimize interference from the radical−radical secondary reactions. In additional one-pass experiments, the temporal profiles of methyl radicals were recorded using UV absorption at 216.5 nm.[48−52]

Several one-pass experiments were performed using absorption of HCO in the visible region at 614.6 nm.[48,53,54]

**Multipass Experiments.** In the multipass arrangement both windows of the cell were replaced by high-reflection dielectric mirrors (CVI corporation), held in angular adjustable mounts. A flat and a concave ($R = 1$ m) mirror composed an optically stable cavity. The manufacturer stated reflectivity of the mirrors at 248 nm was 99.0%, whereas the measured transmittance at 254 nm, the wavelength used in the experiments, was 0.5%. A mercury arc lamp (100 W, Oriel Instruments) was used as a source of the monitoring light at 254 nm. Light from the lamp was focused into the multipass cell using a fused silica lens. The light exiting the cell was passed through two narrow line interference filters (Andover, central wavelength 254 nm, bandwidths 25 nm) mounted on a photomultiplier tube (Hamamatsu R456).

The theory of the multipass cell is described elsewhere.[34] Due to the multiple passing of the absorbing medium, the modulation ($\delta I/I_0$) of the monitoring light intensity increases. The cell "gain", $G$, which is the increase in the modulation compared with the one-pass absorption, is determined by the mirror loss. Actual cell gain was measured using an absorbing species with the absorption coefficient carefully measured in a one-pass geometry. Acetaldehyde was used for this purpose. The gain of the cell was determined using eq 1 (which is valid provided the modulation of light is small):[34]

$$G = -\frac{(\delta I/I_0)}{\sigma l n} \qquad (E1)$$

where $\delta I = I - I_0$, $I$, and $I_0$ are the monitoring light intensities after the cell with and without acetaldehyde added, respectively; $\sigma l = 1.53 \times 10^{-19}$ $cm^3$ $molecule^{-1}$ is the product of the absorption cross section of acetaldehyde at the monitoring wavelength, 254 nm, and the absorption path length; and $n$ is the number density of acetaldehyde molecules. The absorption path length (ca. 10 cm) cannot be precisely determined for the experimental arrangement used. However, because the cell was calibrated using the same carrier and flush gas flows as in the experiments, the only important parameter is the product of the absorption cross-section and the path length, which was accurately measured. The actual cell gain was $78 \pm 8$.

The total flows of the reactant mixtures with helium were in the range 21.7−64 standard cubic centimeter per second (sccs). Additional flush flows to the cold reactor windows were in the range 1.8−2.4 sccs. In the one-pass experiments, the concentrations of the precursors used were $(0.51-2.46) \times 10^{17}$ molecules $cm^{-3}$. The photolysis laser photon fluence was varied in the range $(2.0-25) \times 10^{15}$ photons $cm^{-2}$. The initial concentrations of formyl radicals were in the range $(3.2-78) \times 10^{12}$ molecules $cm^{-3}$. In the multipass cell experiments, the concentrations of the precursors used were $(0.04-0.17) \times 10^{17}$ molecules $cm^{-3}$, and the initial concentrations of formyl radicals were $(7-20) \times 10^{10}$ molecules $cm^{-3}$. The pressure and temperature ranges used in the measurements correspond to the lifetimes of formyl radical in the range 8−1500 $\mu$s in the single-pass experiments, 1−9 ms in the multipass experiments, and 0.8−2.4 ms the CRDS experiments.

**Cavity Ring Down Experiments.** The cavity ring down spectrometer was described previously.[55,56] The light source was a Nd:YAG laser pumped dye laser with a pulse duration of 6−8 ns (manufacturers specification) and a bandwidth of approximately 0.06−0.08 $cm^{-1}$ depending on the wavelength. The bandwidth and the wavelengths were measured by scanning individual rotational lines in the overtone spectrum of water and in the $b^1\Sigma^+ \leftarrow X^3\Sigma^-$ spectrum of $O_2$.

The light leaking out the opposite end of the cavity propagated through two turning prisms, a negative lens, and a sharp cutoff, color glass filter that eliminated shorter wavelength scattered room light, before striking a red-sensitive photomultiplier tube (PMT). A digital card in a computer captured, digitized, and averaged the PMT output. A black aluminum box with a variable aperture for the input beam covered all of the signal collection optics and minimized stray light at the photomultiplier.

The computer was used to analyze the signals and obtain the ring down times. The averaged waveform was transformed to a log(intensity) vs time profile and fit to a line using a linear least squares algorithm. The resulting slope was the inverse of the time constant for the single-exponential decay of light intensity from the cavity. The high-reflectivity mirrors used in this work resulted in an empty cavity ring down time constant ($\tau_0$) between 25 and 35 $\mu$s, depending on the wavelength of the

light and the cell alignment at different temperatures. These $\tau_0$ values correspond to mirror reflectivities of 99.988% and 99.991%.

The apparatus is nearly identical to the one described in the previous paper,[56] with the exception of the inclusion of a photolysis pulse crossing the monitoring beam at a small angle of ca. 1.5° as well as a temperature stabilized heatable flow cell. Second harmonic of a pulse from another Nd:YAG pumped dye laser (320 to 355 nm) was used as photolysis light. The photolysis beam diameter inside the reactor was 4.5 mm, resulting in a 13 ± 3 cm long overlap between the two laser beams, as determined by observation of the two laser spots when the reaction cell was disassembled. The energy of the UV photolysis pulse was 1−2 mJ. The ring down beam passed through the middle of this photolysis volume.

The flow reactor was made of three coaxial Pyrex tubes with the innermost tube of 1.25 cm i.d. Two other tubes formed two jackets that were used to preheat the reaction mixture before entering the photolysis and observation zones. The reaction gas mixture entered through the center of the outermost jacket, exited through two orifices at its ends into the inner jacket and entered the innermost reactor tube through a hole in the center. The reaction flow exited the reactor through two outlets located symmetrically at the distances ±10 cm from the center. The cell had purge volumes at each end. Purge flows were mixed with the reactor flows at the reactor outlets. Therefore, the gas mixture containing precursors and other reactants occupied a length of about 20 cm in the center of the cell. The purge volumes efficiently suppressed exposure of the mirrors to the reaction mixture. The two-jacket arrangement with the distribution of the gas flows described above ensured complete preheating of the gas mixture before entering the reactor. The shorter overlap of the photolysis and the monitoring beams (13 cm) ensured that the HCO kinetics was measured in a well-defined region where temperature was uniform. The reactor was placed in a resistively heated oven. The reactor was incased in two copper semicylinders (38 cm long, 1 mm thick) to ensure better temperature uniformity. The cell was wrapped with a heating tape and several layers of fiberglass insulation. A K-type thermocouple was placed in the thermocouple compartment located in the outer jacket parallel to the reactor axis so that the tip of the thermocouple was located at the center of the reactor. The output of the thermocouple was used to actively stabilize the temperature of the cell. The temperatures in the reaction zone were obtained by measuring the temperature profiles with removable additional thermocouple. The temperature profiles were measured in 2 cm steps along the reactor length separately for each set of the experimental conditions (the temperature set points, total flows and pressures) used in the kinetic measurements. The temperature was uniform (within ±4 K) in the observation zone. This corresponds to the HCO dissociation rate constant uniformity of ±8%.

The overall length of the cell was 95 cm. The total pressures in all kinetic experiments were 0.83 ± 0.01 bar. Calibrated mass flow meters measured the gas flows, which determined the concentrations of the radical precursor and the linear flow velocities of the gases through the reactor. An absorption cell located upstream of the ring down cell was used to measure the concentration of $CH_3CHO$ (HCO radical precursor) via its absorption at 253.6 nm (absorption cross sections $1.51 \times 10^{-20}$ $cm^2$ $molecule^{-1}$).[57]

The experiments on unimolecular decomposition of HCO were performed at three temperatures, 522, 550, and 583 K. Additional experiments were performed at ambient temperature, 298 ± 3 K, to assess the impact of radical recombination and diffusion out of the beam on the kinetic profiles.

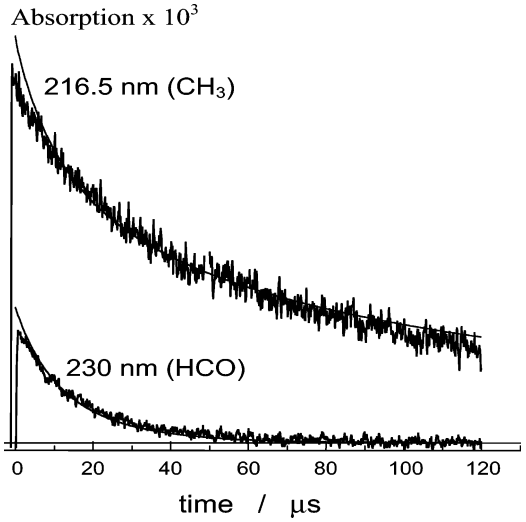


**Figure 3.** Transient absorption profiles at 230 nm (HCO radical) and 216.5 nm ($CH_3$ radical) at 626 K and 1 bar bath gas pressure. Solid lines show the best fit achievable without an adjustment of the rate constant for the reaction of formyl and methyl radicals (see text).

HCO radicals were produced via photolysis of $CH_3CHO$ at 320 nm. Acetaldehyde was supplied in a gas flow using a bubbler containing liquid acetaldehyde at −56 °C. The carrier gas, which served as the major bath gas, as well as the carrier of acetaldehyde vapor, was passed through two oxygen filters in series (Restek high-capacity oxygen trap, #20610, manufacturer stated oxygen content reduction to 15 ppb) before entering the reactor to remove $O_2$, which reacts rapidly with HCO. Originally used Teflon tubing was replaced by copper tubing. This was done to prevent oxygen diffusing through Teflon tubing into the reactor from the atmosphere. This replacement resulted in a substantial increase in the lifetime of HCO radicals (from ca. 1.5 ms to ca. 10 ms at 300 K).

The delay between photolysis and the ring down laser was controlled by a home-built, computer-controlled device. The software provided random generation of the delay times to avoid any systematic distortions of the kinetic profile due to any drifts in CRDS detection sensitivity. The repetition rate of the lasers was 1 Hz and, thus, ensured complete replacement of the gas mixture between the pulses.

## Results and Discussion

**One-Pass Experiments.** Transient absorption profiles were measured at fourteen combinations of temperature and pressure. Examples of measured temporal profiles of absorption at 230 nm (HCO radical) and at 216.5 nm ($CH_3$ radical) are shown in Figure 3. For the qualitative assessment of the contributions of radical−radical processes to the measured decay profiles the following approach was used. The temporal absorption profiles were fitted by an exponential decay function. The decay parameters (the apparent rate constants) were determined at several laser energies. Extrapolation of the apparent rate constants to zero initial radical concentration (zero initial absorption) was used to estimate the rate constant of reaction 1 and the contribution of radical−radical reactions. An example is shown in Figure 4.

To determine the rate constant of reaction 1, a reaction mechanism described below was used to model and fit the experimental profiles. Absorption profiles at 230 nm (HCO absorption) and 216.5 nm (mainly $CH_3$ absorption) were

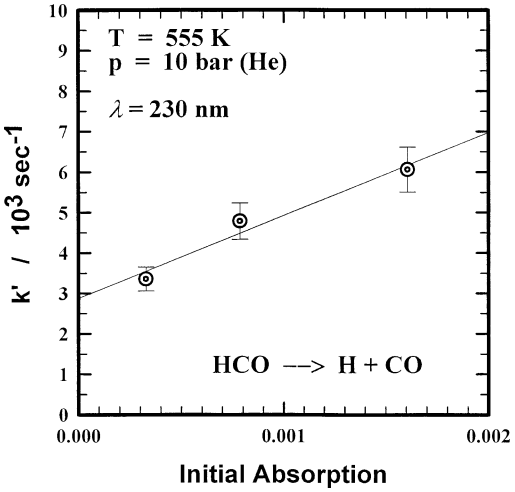


**Figure 4.** Extrapolation of the apparent rate constant to zero initial concentration of formyl radicals (555 K, 10 bar, He) to illustrate the relative role of radical−radical reactions.

recorded at two different laser pulse energies. All four profiles obtained were simultaneously fitted by a numerical solution of a system of differential equations corresponding to the reaction mechanism. The reaction mechanism used in the fits included reaction 1 and additional reactions 4−10:

$$CH_3 + HCO \rightarrow CH_4 + CO \quad (4a)$$

$$\rightarrow CH_3CHO \quad (4b)$$

$$HCO + HCO \rightarrow H_2CO + CO \quad (5a)$$

$$\rightarrow (HCO)_2 \quad (5b)$$

$$\rightarrow CO + CO + H_2 \quad (5c)$$

$$CH_3 + CH_3 \rightarrow C_2H_6 \quad (6)$$

$$CH_3 + CH_3CHO \rightarrow CH_4 + CH_3CO \quad (7a)$$

$$\rightarrow C_2H_6 + HCO \quad (7b)$$

$$H + CH_3CHO \rightarrow H_2 + CH_3CO \quad (8a)$$

$$\rightarrow CH_4 + HCO \quad (8b)$$

$$H + HCO \rightarrow H_2 + CO \quad (9a)$$

$$\rightarrow H_2CO \quad (9b)$$

$$CH_3CO \rightarrow CH_3 + CO \quad (10)$$

The UV absorption cross-sections and the rate constants, used in the fits, were ether measured in the current work (e.g., absorption of acetaldehyde, revised absorption cross-section of HCO, and rate constants of reactions 4 and 5[32,58,59]) or taken from the literature. In the initial fits, the rate constants of reactions 4−10 were taken from the NIST Kinetics database.[60] Reactions of unimolecular dissociation of $CH_3CO$ (reaction 10), as well as those of $C_2H_5CO$ and $C_2H_5$ radicals (formed when photolysis of propionaldehyde, $C_2H_5CHO$, was used as a source of HCO radicals) are fast and are completed on a time scale much shorter than the time scale of the thermal dissociation of HCO. Reaction 8 is also fast under our experimental conditions. Therefore, hydrogen atoms are in steady-state with HCO radicals. Modeling results show that the steady-state concentration of H atom is 2 orders of magnitude lower and the steady-state concentration of $CH_3CO$ radicals is 3 orders of magnitude lower than that of HCO radicals. Therefore, the radical−radical processes involving H atoms and $CH_3CO$ radicals can be neglected. The temporal behavior of formyl radicals is primarily controlled by their unimolecular dissociation (1), self-reaction (5), and reaction with methyl radicals (4).

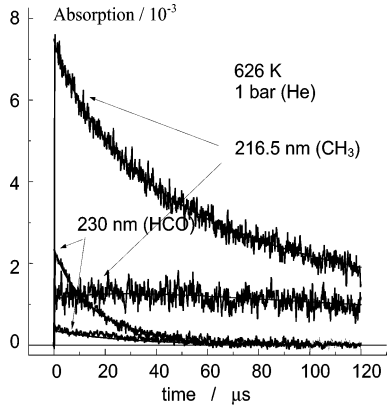


**Figure 5.** Transient absorption profiles at 230 nm (HCO radical) and 216.5 nm ($CH_3$ radical) recorded at different laser pulse energies (626 K, 1 bar, He). The solid lines show the results of the simultaneous fit of the four profiles with an adjusted rate constant for the reaction of methyl and formyl radicals (see text).

At first, only the initial concentrations of formyl radicals and the rate constant of reaction 1 were used as fitting parameters. The results of the fits were as follows: First, the fits were completely insensitive to the separation of reactions 4 and 5 into separate channels (due to the nonradical nature of the products and negligible absorption at the monitoring wavelength by the products of these reactions). Second, the fits showed minimal sensitivity to the rate constants of reactions 8−10 (except for the branching ratio $a_{8b}$ in reaction 8, where HCO is formed). This is because reactions 8 and 10 are fast, and reaction 9 contributes only a few percent in the consumption of hydrogen atoms. Third, no satisfactory fits could be achieved without adjusting the cross-section of the HCO radical at 230 nm and using rate constants for the reactions of methyl and formyl radicals (reaction 4) that are different from the recommended literature values. Good fits were obtained when the rate constant of reaction 4 was reduced to $(0.5-1.3) \times 10^{-10}$ cm$^3$ molecule$^{-1}$ s$^{-1}$ (about a factor of 2−3 lower than the recommended value, $2 \times 10^{-10}$ [60]) and the absorption cross section of HCO radical at 230 nm was increased from $3.5 \times 10^{-18}$cm$^2$ (reported by Hochandanadel et al.[47]) to $(7-9) \times 10^{-18}$ cm$^2$. In the original work of Hochandanadel et al. [47] the absorption spectrum of HCO was obtained in a chemical system, where HCO radicals were formed via recombination of hydrogen atoms with CO molecules. Their analyses included a fairly complicated reaction mechanism. Because the fits suggested that the literature absorption cross-sections and the rate constant of HCO with methyl radical could be in error, an additional study was performed to address these issues.[32,58,59] Direct measurements of the HCO absorption cross section at 230 nm, based on the quantitative measurements of the photon flux of the photolysis light yielded $\sigma_{230}(\mathrm{HCO}) = (7.5 \pm 1.2) \times 10^{-18}$ cm$^2$ molecule$^{-1}$ at 588 K[58] and new rate constants for reaction 4: $(9.9 \pm 1.9) \times 10^{-11}$ at 298 K and $(8.6 \pm 2.2) \times 10^{-11}$ cm$^3$ molecule$^{-1}$ s$^{-1}$ at 591 K.[32,58,59] The results of the fits using reactions 1 and 4−10 with the adjusted cross-section for HCO and the rate constant of reaction 4 are illustrated in Figure 5. The experimental conditions and the measured first-order rate constants of reaction1 are summarized in Table 1.

**TABLE 1: Rate Constant for the HCO → H + CO Reaction**

| $T$/K[a] | $p$/bar | total flow, sccs | $[CH_3CHO]/10^{17}$ molecules cm$^{-3}$ | method[b] | $k_1'/10^3$ s$^{-1}$ [c] | $k_{1,bi}/10^{-17}$ [d] cm$^3$ molecule$^{-1}$ s$^{-1}$ ($k_{1,bi} = k_1'/[He]$) |
|---|---|---|---|---|---|---|
| 669 | 1.0 | 21.7 | 0.75 | UV-SP | 7.0 ± 1.0 | 65 ± 9 |
| 769 | 1.0 | 21.7 | 0.65 | UV-SP | 29.4 ± 3.5 | 312 ± 36 |
| 769 | 1.5 | 26 | 1.01 | UV-SP | 38.5 ± 4.4 | 273 ± 32 |
| 669 | 10 | 43.5 | 1.25 | UV-SP | 54.9 ± 6.1 | 51 ± 6 |
| 626 | 10 | 43.5 | 1.34 | UV-SP | 22.7 ± 2.6 | 19.6 ± 2.3 |
| 715 | 10 | 44.3 | 1.73 | UV-SP | 120 ± 7 | 118 ± 8 |
| 588 | 10 | 43.5 | 1.42 | UV-SP | 8.0 ± 1.0 | 6.5 ± 0.9 |
| 555 | 10 | 64 | 0.51 | UV-SP | 2.9 ±0.7 | 2.2 ± 0.5 |
| 587 | 30 | 21.5 | 1.4 | UV-SP | 22.2 ± 2.5 | 6.0 ± 0.7 |
| 715 | 1.0 | 24 | 0.89 | UV-SP | 10.5 ± 1.7 | 104 ± 17 |
| 626 | 1.0 | 24 | 1.01 | UV-SP | 3.03 ± 0.41 | 26.2 ± 3.6 |
| 588 | 1.0 | 24 | 1.08 | UV-SP | 0.69 ± 0.12 | 5.6 ± 1.0 |
| 575 | 100 | 41 | 2.46 | UV-SP | 48.8 ± 5.8 | 3.9 ± 0.5 |
| 575 | 100 | 41 | 2.46 | UV-SP | 47.2 ± 5.6 | 3.7 ± 0.5 |
| 498 | 1.01 | 22 | 0.043−0.17 | UV-MP | 0.115 ± 0.015 | 0.78 ± 0.14 |
| 575 | 1.01 | 22 | 0.073 | UV-MP | 0.99 ± 0.15 | 7.8 ± 1.2 |
| 522 | 0.82 | 20 | 0.059−0.19 | Red-CRDS | 0.36 ± 0.12 | 3.2 ± 0.8 |
| 550 | 0.82 | 20 | 0.060 | Red-CRDS | 0.57 ± 0.15 | 5.3 ± 1.1 |
| 583 | 0.82 | 20 | 0.062 | Red-CRDS | 1.18 ± 0.16 | 11.6 ± 1.3 |

[a] Temperature uncertainty ±5 K. [b] UV-SP: single pass absorption at 230 nm. UV-MP: multipass absorption at 254 nm. Red-CRDS: cavity ring down spectroscopy at 613.817 nm. [c,d] The errors are ±3 standard deviations and reflect statistical accuracy only.

Several additional measurements were performed using the "red" transition of the HCO radical (at 614.7 nm) using the single-pass system. The average absorption (over the slit function 1 nm) at this wavelength is much lower than that in the UV, and the kinetic profiles were of much lower quality. Yet qualitatively, the results of such experiments were in accord with those from UV measurements (in the sense that they confirmed longer lifetime of HCO radical compared to the literature data). Due to the large error in the decay parameters obtained in these measurements, results from the single-pass measurements at 614.7 nm are not included in the final data set.

At low temperatures, when the lifetime of the HCO radical is longer than 1 ms, very low concentrations of HCO are required to make the contribution of radical−radical reactions small compared to its unimolecular decay due to reaction 1. At these temperatures, the sensitivity of the one pass absorption technique was not sufficient and the highly sensitive multipass absorption technique as well as cavity ring down spectroscopy was used.

Experiments using the multipass cell were performed at ambient and two elevated temperatures, 498 and 588 K, and a pressure of 1 bar (He). The initial concentrations of HCO in these experiments were $(0.7-2.0) \times 10^{11}$ molecules cm$^{-3}$. At 588 K the apparent decay time was 1.02 ± 0.15 ms at the initial concentration of HCO radicals of $1 \times 10^{11}$ molecules cm$^{-3}$; the contributions of radical−radical reactions were negligible (ca. 2%). At 498 K, however, the apparent decay time varied between 6.5 and 8 ms in experiments with the different initial concentrations of HCO. For these experiments, numerical modeling using the mechanism consisting of reactions 1 and 4−10 (discussed above) was used, where only the initial concentrations of HCO and the rate constant of reaction 1, $k_1$, were used as fitting parameters. The modeling yielded 8.7 ± 0.9 ms for the lifetime of HCO with respect to the dissociation at 498 K. The results are summarized in Table 1.

The experiments using cavity ring down spectroscopy at the red transition of HCO radical were performed at ambient and three elevated temperatures 583, 550, and 522 K, at 0.82 bar (He). An example of the measured HCO decay is shown in Figure 6. Typical concentrations of HCO in these experiments were $(0.7-4) \times 10^{11}$ molecules cm$^{-3}$. The measured apparent decay time constants were 0.8, 1.59, and 2.37 ms at 583, 550, and 522 K, respectively. The estimated contributions of the radical−radical reaction were respectively only ca. 1%, 2%, were and 4%. However, due to the long lifetimes and relatively small diameter of the photolysis beam, radial diffusion of HCO radicals made a noticeable contribution to the absorption decay. The diffusion coefficient of HCO in He was estimated using the Wilke−Lee method.[61] The Lennard-Jones diameter of HCO, $\sigma_{HCO} = 0.349$ nm was estimated using the Le Bas additive volume increments of C, O, and H, $V_{b,HCO} = 25.9$ cm$^3$ mol$^{-1}$. The parameter $\epsilon_{HCO}/k_B = 424$ K was estimated using the relation $\epsilon/k = 1.15T_b$. The boiling temperature, $T_b$, was taken as that of $H_2CO$, i.e., $T_b(HCO) = T_b(H_2CO) = 369$ K. The parameters for helium ($\sigma_{He} = 0.2551$ nm, $\epsilon_{He}/k_B = 10.22$ K were taken from the literature (Table C[61]). The Lennard-Jones parameters for the pair HCO−He were obtained using the standard combination rules,[61] ($\sigma_{HCO-He} = 0.302$ nm, $\epsilon_{HCO-He}/k_B = 65.8$ K). The diffusion coefficients calculated at different temperatures were fitted to eq E2 for 250−3000 K.

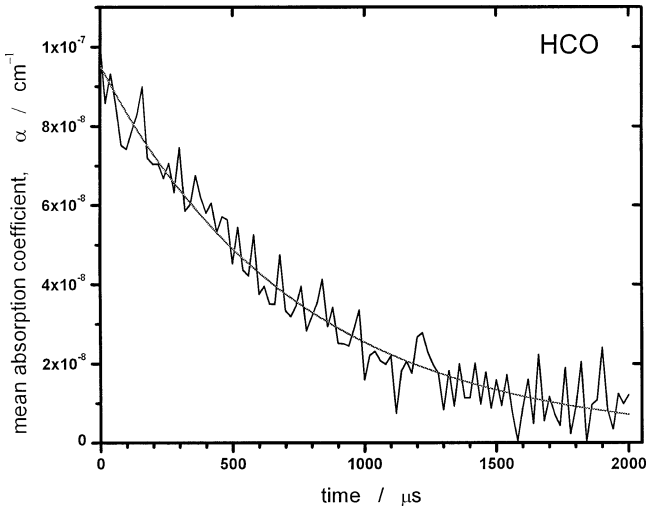


**Figure 6.** Sample temporal profile of HCO radical obtained using cavity ring down spectroscopy (CRDS) at 613.817 nm. Temperature: 583 K. Pressure: 613 Torr (He). Photolysis of acetaldehyde at 320 nm.

$$D_{HCO-He} = 0.67(T/298)^{1.67} \text{ cm}^2 \text{ s}^{-1} \text{ (1 atm)} \qquad \text{(E2)}$$

**TABLE 2: Diffusion Coefficients for HCO in He and Calculated Corrections for the Apparent Decay Constants in the CRDS Experiments**

| $p$/bar | $T$/K | $D_{HCO-He}$/cm$^2$ s$^{-1}$ [a] | $2D/R^2$, s$^{-1}$ [b] | $k_{app}$/s$^{-1}$ [c] | $k'_{app}$ [d] | $k'_{est}$ [e] | $k'_{D,app}$ [f] | $k_{D,app}$ [g]/s$^{-1}$ | corrected [h] k/s$^{-1}$ |
|---|---|---|---|---|---|---|---|---|---|
| 0.82 | 298 | 0.82 | $32 \pm 10$ | | | | | | |
| 0.82 | 522 | 2.12 | $84 \pm 25$ | $422 \pm 69$ | 5.02 | 4.35 | 0.69 | $58 \pm 17$ | $364 \pm 86$ |
| 0.82 | 550 | 2.32 | $92 \pm 28$ | $630 \pm 90$ | 6.85 | 6.18 | 0.67 | $62 \pm 19$ | $568 \pm 109$ |
| 0.82 | 583 | 2.56 | $101 \pm 30$ | $1247 \pm 96$ | 12.34 | 11.67 | 0.62 | $63 \pm 19$ | $1184 \pm 115$ |

[a] Calculated; see text for details. [b] The errors are due to the uncertainty in the diffusion coefficients and the beam geometry (see text). [c] The apparent first-order decay rate constant, the errors are $\pm 3$ standard deviations. [d] The dimensionless apparent first-order rate constant, $k'_{app} = k_{app}/(2D/R^2)$. [e] An estimate on the dimensionless decay constant, $k'_{est} = k'_{app} - 0.67$ (see Appendix). [f] The dimensionless apparent contribution to the decay due to the out-of-beam diffusion, obtained using Table 3 from Appendix. [g] The apparent diffusion contribution to the decay, $k_{D,app} = k'_{D,app}(2D/R^2)$. [h] The corrected decay rate constant, $k = k_{app} - k_{D,app}$.

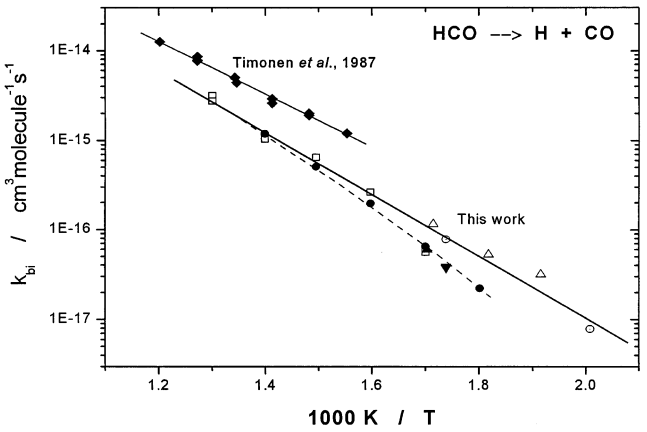


**Figure 7.** Arrhenius plot of the bimolecular rate constant for reaction HCO → H + CO (reaction 1): (◆) previous direct measurements.[15] Open symbols: 1 bar, this work [(□) transient UV, one-pass; (○) transient UV, multipass; (△) CRDS, red transition of HCO]. Filled symbols: this work, transient UV absorption, one pass; (●) 10 bar; (▲) 30 bar; (▼) 100 bar.

The measured HCO profiles were corrected for the radial radical diffusion as follows. The diffusion problem was solved explicitly (see Appendix). Cylindrically symmetric uniform initial distribution of absorbing molecules (HCO) was assumed in the calculations. The initial diameter of this distribution was taken to be 0.45 cm, the photolysis beam diameter in the reactor. The calculated diffusion coefficients at the experimental conditions used are listed in Table 2 together with the diffusion corrections and the corrected rate constants for the unimolecular decomposition of HCO radical. The diffusion corrections varied from 14% to 5% of the decay constant in the temperature range 522−583 K. We estimate the uncertainty of the diffusion correction as ±30% of the correction itself due to the uncertainties both in the evaluated diffusion coefficients and in the evaluated beam geometry. The out-of-beam diffusion problem itself was solved exactly.

The experimental results together with the results of the previous direct study are shown in Figure 7. The solid line is linear regression drawn through the points taken at 1 bar pressure. The second-order rate constant obtained by a linear regression in the Arrhenius coordinates (ln($k$) vs $T^{-1}$) from the data at 1 bar is

$$k_1(\mathrm{He}) = (0.8 \pm 0.4) \times 10^{-10} \exp(-66.0 \pm 3.4 \text{ kJ mol}^{-1}/RT) \text{ cm}^3 \text{ molecule}^{-1} \text{ s}^{-1} \quad (\mathrm{He}, 498-769 \text{ K}) \quad (E3)$$

The dissociation rate constants measured in this work are systematically and consistently lower than those reported in the previous direct work.[15] The difference is a factor of 2.2 at the highest temperature and a factor of 3.5 at the lowest temperature of our experiments. This is a significant discrepancy of potential importance in combustion modeling, as well as in the theoretical treatment of reaction 1.

We performed a number of checks to verify our results. Several experiments were done using the red transition of the radical (at 614.6 nm) as well as a different precursor molecule ($C_2H_5CHO$). These measurements were in accord with the results obtained using acetaldehyde and UV transition of the radical.

Almost all hypothetical interfering processes (such as radical−radical reactions) would lead to an *increase* of the measured rate constant. The only one possibility for an interfering process that leads to a *decrease* of the apparent rate constant is the regeneration of formyl radicals (via reactions such as (7b) and (8b)). Very little is known about these channels of reactions 7 and 8. To check for such a possibility, acetaldehyde was photolyzed at 193 nm to evaluate the role of the secondary reaction of methyl radicals and hydrogen atoms with the precursor molecule. Acetaldehyde has negligible absorption at 193 nm at ambient temperature. However, strongly temperature dependent "hot band" absorption of acetaldehyde has been predicted and was experimentally found in the current study. Over the temperature range 570−770 K the absorption cross-section was $(0.2-4.0) \times 10^{-20}$ cm$^2$ molecule$^{-1}$. The major route of acetaldehyde photodissociation at 193 nm is production of methyl radical and hydrogen atom (11a); formation of a small amount of formyl radicals (11b) cannot be ruled out:

$$CH_3CHO + h\nu(193 \text{ nm}) \rightarrow CH_3 + H + CO \quad (11a)$$

$$\rightarrow CH_3 + HCO \quad (11b)$$

By measuring the amplitude of the HCO radicals absorption in comparison with the absorption of methyl radicals in photolysis of acetaldehyde at 193 nm, an upper limit on the possible fraction of formyl radicals produced in the reactions of hydrogen atoms and methyl radicals with acetaldehyde and other reactions could be estimated. These measurements yielded a ratio of the maximum concentration of formyl radicals to methyl radicals of 0.12. Because this includes possible production of formyl radicals through channel 11b, it gives an *upper limit* of 12% for the possible regeneration of formyl radicals from both *hydrogen atoms* and *methyl radicals*. A better limit on the possible reproduction of HCO via the reaction of *hydrogen atoms* with acetaldehyde (channel 8b) was obtained in the CRDS experiments. In these experiments, $Cl_2/H_2/CH_3CHO$ mixtures ($H_2$ was used as a carrier gas) were photolyzed at 350 and 355 nm. Under the conditions used, chlorine atoms were quickly converted to hydrogen atoms in reaction with molecular hydrogen, which was added in great excess:

$$Cl_2 + h\nu(350\ nm) \rightarrow Cl + Cl \quad (12)$$

$$Cl + H_2 \rightarrow HCl + H \quad (13)$$

$$H + Cl_2 \rightarrow HCl + Cl \quad (14)$$

Formation of HCO radicals was monitored by CRDS at 613.8 nm after a fixed delay of 250 $\mu$s (which corresponds to the maximum concentration of HCO established on the basis of the modeling). In addition, temporal profiles of the CRDS signals were recorded. Typical concentrations in these experiments were $[H_2] = 2 \times 10^{19}$ cm$^{-3}$, $[Cl_2] = 4 \times 10^{14}$ cm$^{-3}$, and $[CH_3CHO] = 6 \times 10^{15}$ cm$^{-3}$. Under such conditions, the characteristic time for reaction 13 is less than 120 ns. This reaction converts chlorine atoms into hydrogen atoms almost quantitatively (reaction of chlorine atoms with acetaldehyde contributes only ca. 4%). A reaction mechanism was used to model the HCO profiles. The mechanism included reactions 1 and 4−14 and, additionally, reactions 15−21:

$$CH_3CO + Cl_2 \rightarrow CH_3ClCO + Cl \quad (15)$$

$$CH_3 + Cl_2 \rightarrow CH_3Cl + Cl \quad (16)$$

$$Cl + CH_3CHO \rightarrow HCl + CH_3CO \quad (17)$$

$$HCO + Cl_2 \rightarrow HClCO + Cl \quad (18)$$

$$HCO + H_2 \rightarrow H_2CO + H \quad (19)$$

$$CH_3 + H_2 \rightarrow CH_4 + H \quad (20)$$

$$CH_3CO + H_2 \rightarrow CH_3CHO + H \quad (21)$$

In the modeling, the branching ratio in reaction 8, $f_{8b} = k_{8b}/(k_{8a} + k_{8b})$, was varied. The "conversion efficiency of chlorine atoms", the ratio of the maximum concentration of HCO radical to the product of the initial concentration of chlorine atoms and the branching ratio $F = [HCO]_{max}/([Cl]_0 f_{8b})$, was determined. Under the experimental conditions used, this ratio was in the range 0.5−0.6. The initial concentration of chlorine atoms (typically $5 \times 10^{11}$ molecules cm$^{-3}$) was estimated on the basis of the UV beam energy density, absorption cross-section of chlorine molecules, and the geometry of the photolysis and the monitoring beam. The amplitudes of the CRDS signals of HCO appearing in photolysis of the $Cl_2/CH_3CHO/H_2$ mixtures at 350 nm were compared with the amplitudes of HCO signals in the photolysis of $CH_3CHO$ at 320 nm. The UV photolysis fluence was measured in all experiments. Finally, an estimate on the branching ratio $f_{8b}$ was obtained on the basis of the ratios of the CRDS signals of HCO, $[HCO]_{350}/[HCO]_{320}$, the "conversion efficiency of chlorine atoms", $F = 0.5-0.6$, the ratio of the pulse energies at 320 and 350 nm, $E_{320}/E_{350}$, the reactants concentrations, and the ratio of the absorption cross-sections and the quantum yields of chlorine atoms and HCO radicals in photolysis of molecular chlorine and acetaldehyde, $\sigma_{350}(Cl_2)\phi_{350}(Cl)/\sigma_{320}(CH_3CHO)\phi_{320}(HCO)$:

$$f_{8b} \le \frac{[HCO]_{350}E_{320}[CH_3CHO]\sigma_{320}(CH_3CHO)\phi_{320}(HCO)}{F[HCO]_{320}E_{350}[Cl_2]\sigma_{350}(Cl_2)\phi_{350}(Cl)} \quad (E4)$$

In the estimates, the quantum yields were taken as $\phi_{350}(Cl) = 2$, $\phi_{320}(HCO) = 0.1$.[62] The measurements led to an upper estimate on the branching ratio in reaction 8:

$$f_{8b} < 0.002 \quad (E5)$$

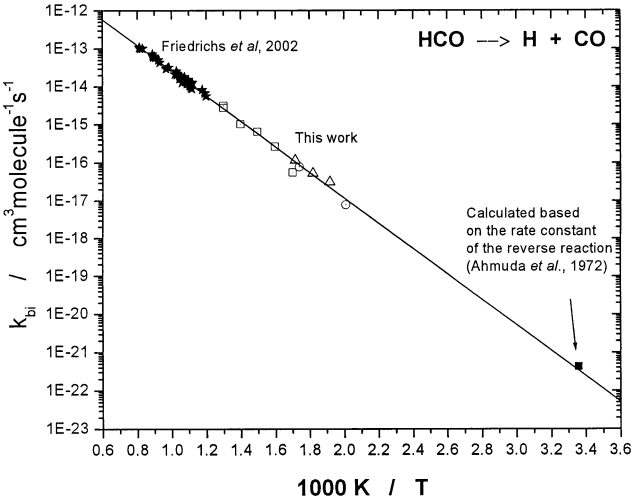


**Figure 8.** Arrhenius plot of the bimolecular rate constant for reaction HCO → H + CO (reaction 1) over an extended temperature range. Open symbols: this work, 1 bar [(□) transient UV, one-pass; (○) transient UV, multipass; (△) CRDS, red transition of HCO]. (■) Calculated from the rate constant of the reverse reaction, H + CO → HCO[22] using the most recent thermochemical data.[6] (★) Shock tube measurements of Friedrichs et al.[63] The solid line is a linear regression drawn through all these points.

However, experiments with the photolysis of $CH_3CHO$ alone at 350 nm (without chlorine and hydrogen) did show CRDS signals of HCO at 521 K (the temperature of the experiments described above). The signal amplitude suggests that the whole HCO signal observed in the photolysis of $Cl_2/CH_3CHO/H_2$ mixtures at 350 nm can be attributed to photolysis of acetaldehyde. Therefore, the estimate (E5) should be considered as an upper estimate and does not suggest any yield of HCO radicals in reaction of hydrogen atoms with acetaldehyde.

From Figure 7, the deviation of the "high-pressure" points from those measured at 1 bar, is apparent. This effect is more pronounced at low temperatures, as can be expected in the case of a pressure falloff. Such an earlier pressure falloff was theoretically predicted on the basis of the theory of isolated resonances.[15] No noticeable deviations from the second order (and consequently no pressure dependence of the second-order rate constant) are expected for reaction 1 over the pressure and temperature ranges of this study based on the classical RRKM theory.[14] Because only limited high-pressure data were obtained, the assignment of the deviation of the high-pressure points to the earlier falloff caused by the nonstatistical nature of HCO should be considered as tentative.

The rate constant of reaction 1 can be calculated from the rate constant of the reverse reaction (−1) and the equilibrium constant. The thermochemistry of reaction 1 is known with high accuracy.[6] The rate constant of reaction 1 at ambient temperature, calculated using the rate constant of reaction of hydrogen atoms with carbon dioxide (the only direct study where helium was used as a bath gas[22]) and the thermochemical data,[6] is shown in Figure 8 together with the current measurements. This calculated rate constant is in good agreement with the extrapolated low-pressure value measured in this work.

Recently, rate constants of reaction 1 were measured using the shock tube technique at pressures around 1 bar over the temperature range 835−1230 K.[63] The results are in excellent agreement with the results of the current study. The low-pressure data of the current study, together with the shock-tube data and the low-temperature point obtained from the reverse reaction (via thermochemistry and the rate constant of the reverse

reaction) are shown in Figure 8. A simple two-parameter Arrhenius expression fits all the data well. The fit yields:

$$k_1(\mathrm{He}) = (0.60 \pm 0.14) \times 10^{-10} \exp(-64.2 \pm 1.4 \text{ kJ mol}^{-1}/RT) \text{ cm}^3 \text{ molecule}^{-1} \text{ s}^{-1} \quad (\mathrm{He}, 298-1229 \text{ K}) \quad \text{(E6)}$$

An attempt was made to identify possible sources of error in the previous direct study of reaction 1 using laser photolysis to produce HCO and photoionization mass spectrometry to detect it (LP PIMS).[15] Analysis of the experimental conditions and the experimental procedures used in their study did not reveal any flaws as far as the *homogeneous* gas-phase reactions are concerned. The main concern is the fate of hydrogen atoms produced in reaction 1, and the relative role of the possible subsequent reaction of these atoms with HCO radicals:

$$\mathrm{H} + \mathrm{HCO} \rightarrow \mathrm{H_2} + \mathrm{CO} \quad (22)$$

The initial concentrations of free radicals were kept sufficiently low to make contributions of this reaction as well as of other possible radical−radical reactions negligible. However, low initial concentrations of HCO radicals do not preclude a possibility of HCO radical undergoing *heterogeneous* reaction with a hydrogen atom absorbed on the wall of the flow tube, H(s):

$$\mathrm{H} \rightarrow \mathrm{H(s)} \quad (23)$$

$$\mathrm{HCO} + \mathrm{H(s)} \rightarrow \mathrm{H_2} + \mathrm{CO} \quad (24)$$

Alternatively, adsorption of the HCO radical with subsequent reaction with the adsorbed H atom is also possible. In a study of H-atom decay on the CVD diamond surface,[64] it was observed that boric acid (and boron oxide, produced from decomposition of boric acid at elevated temperatures[65]) exhibits high catalytic activity for heterogeneous recombination of hydrogen atoms, so that a different passivation technique was required to reduce the catalytic activity of the flow tube wall. It was also observed that H-atom decay was through a recombination process to produce molecular hydrogen quantitatively. Boric acid was used as a wall coating in the LP PIMS study.[15] It could be speculated that hydrogen atoms accumulated on the surface so that the surface coverage was sufficient to balance their generation in reaction 1 and consumption in reaction 24. This mechanism could lead to the doubling of the consumption rate of HCO radicals, and, subsequently, to a 2-fold increase of the measured apparent decay constant. However, this is merely a suggestion for explanation of the observed discrepancy.

## Conclusions

Unimolecular dissociation of formyl radicals was studied over an extended buffer gas pressure range. The dissociation rate constants measured in this work are lower than those reported in the previous direct study. The difference is a factor of 2.2 at the highest temperature of the experiments and a factor of 3.5 at the low end. This discrepancy is of potential importance in combustion modeling and in the theoretical treatment of reaction 1. Pressure dependence of the rate constant of the reaction was found and is attributed to the pressure falloff expected on the basis of the theory of isolated resonances.[14]

**Acknowledgment.** This work was partially supported by the Petroleum Research Fund administered by the American Chemical Society (Grant No. 31640-AC6). Work at NOAA was funded by NOAA's Health of the Atmosphere Research Program.

## Appendix

Correction for the diffusion of HCO out of the detection beam in the CRDS experiments is considered here. The diffusion equation is solved for an axially symmetric diffusion of molecules probed by a much narrower beam crossing the photolyzed region at an arbitrary angle.

An axially symmetric initial distribution of the transient molecules of interest is created by a photolysis pulse (or by any other means). The monitoring light beam crosses the photolysis beam in such a way that the axes of the two beams intersect (at an arbitrary angle). In the derivation below, it is assumed that the monitoring beam is much narrower than the photolysis beam.

Notations: $z$ is the direction of the photolysis beam, $x$ is the axis in the plane of the two beams perpendicular to $z$, and $y$ is perpendicular to $z$ and the plane of the two beams, and $r$ the distance from a point to the axis of the photolysis beam. Then, the absorption of the monitoring beam is given by

$$\mathrm{Abs} = (2\sigma/\sin(\alpha))\int_0^\infty n(r,t)\, \mathrm{d}r \quad \text{(A1)}$$

Introducing the Green function, $G$ (the solution of the diffusion problem for the infinitely thin beam parallel to the photolysis beam but shifted relative to the photolysis beam axis by $x'$ and $y'$):

$$G(x,x',y,y',t) = (4Dt\tau)^{-1} \exp(-(x-x')^2/4Dt) \exp(-(y-y')^2/4Dt) \quad \text{(A2)}$$

Then, for an arbitrary initial distribution $n_0(x',y')$, one derives

$$n(x,y,t) = \int\int n_0(x',y')\, G(x,x',y,y',t)\, \mathrm{d}x'\, \mathrm{d}y' \quad \text{(A3)}$$

Substituting the Green function A2 and assuming uniform initial distribution of absorbing molecules within the cross-section of the photolysis beam of radius $R$ with the density $n_0$ into A3, and combining with the eq A1, one obtains:

$$\mathrm{Abs} = (2\sigma n_0/\sin(\alpha))(4Dt\tau)^{-1} \int_{x'^2+y'^2 \le R^2} \exp\left(-\frac{(x-x')^2}{4Dt}\right) \exp\left(-\frac{(y-y')^2}{4Dt}\right) \mathrm{d}x'\, \mathrm{d}y' \quad \text{(A4)}$$

Integrating first over $x$, and then over $x'$, yields

$$\mathrm{Abs} = (2\sigma n_0/\sin(\alpha))(4Dt\tau)^{-1/2} \int_0^R \exp\left(\frac{-y'^2}{4Dt}\right) \sqrt{(R^2-y'^2)}\, \mathrm{d}y' \quad \text{(A5)}$$

Analysis of eq A5 shows that $\mathrm{Abs}_0 = 2\sigma n_0/\sin(\alpha)$ is the initial absorption. Introducing the dimensionless time, $t' = 2Dt/R^2$, and the dimensionless radius, $\rho = r/R$, eq A5 becomes eq A6:

$$\mathrm{Abs}/\mathrm{Abs}_0 = f_D(t') = \frac{2}{\pi t'} \int_0^1 \exp\left(\frac{-\rho^2}{2t'}\right) \sqrt{(1-\rho^2)}\, \mathrm{d}\rho \quad \text{(A6)}$$

This equation contains only dimensionless time, $t' = 2Dt/R^2$.

It could be shown[66] that the diffusion kinetics precisely factors out from the reaction contribution provided that the chemical reaction of the monitored species obeys first-order law. In other

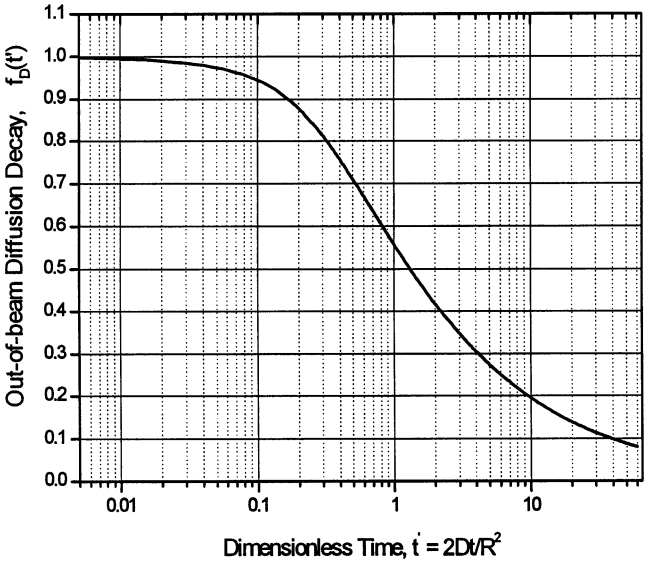


**Figure 9.** Universal dimensionless decay function $f_D(t')$ due to the out-of-beam diffusion for a thin monitoring beam crossing a uniform axially symmetric initial distribution of absorbing particles within the radius $R$. The dimensionless time is $t' = 2Dt/R^2$.

words, the decay profile is the product of the diffusion decay profile and the decay profile due to the chemical reactions without diffusion. Therefore, for first-order reactions the diffusion correction can be obtained separately, on the basis of eq A6. The diffusion kinetics is nonexponential, and the value of the "apparent diffusion constant", $k_{D,app}$, depends on the depth of the decay caused by the diffusion solely over the time range in which the kinetics is fitted by a first-order (exponential) function. The integral in (A6) was numerically evaluated for different dimensionless times, and the "diffusion decay profile", $f_D(t')$, was calculated. The graph of $f_D(t')$ is shown in Figure 9.

Because the diffusion kinetics is nonexponential, no single "diffusion decay constant" can be derived. The contribution of the diffusion in the decay depends on the ratio of the decay rate due to the chemical reactions and the characteristic diffusion parameter, $2D/R^2$. For different dimensionless decay constants, $k$, decay profiles due to combined diffusion and reaction were calculated:

$$F(t') = f_D(t') \exp(-k't') \qquad \text{(A7)}$$

These profiles were fitted by simple exponential decay, $F_{fit}(t')$:

$$F_{fit}(t') = A \exp(-k'_{app}t) \qquad \text{(A8)}$$

The resulting dimensionless first-order apparent rate constant, $k'_{app}$, for different $k'$ and the fitting interval, are listed in Table 3. In addition, the difference between the apparent and the original first-order rate constant, which is associated with the diffusion contribution to the decay constant, $k'_{D,app}$, is calculated.

The numerical simulations show that over the range of $k'$ from 0.2 to 40 ($0.2 \le k/(2D/R^2) \le 40$), the apparent contribution of the out-of-beam diffusion to the apparent decay constant is within 47−69% of the $2D/R^2$:

$$k_{D,app} = (0.47-0.69)2D/R^2 \qquad \text{(A9)}$$

Equation A9 can be used to roughly estimate the contribution of the out-of-beam diffusion for the crossing beam geometry and the uniform cylindrical initial distribution. To obtain accurate corrections, the exact results (Table 3) should be used.

**TABLE 3: Apparent Dimensionless First-Order Decay Parameter, $k'_{app}$, the Apparent Amplitude, $A$, and the Apparent Dimensionless Out-of-Beam Diffusion Contribution, $k'_{D,app}$, for Different Dimensionless Decay Parameters, $k'$, and the Fitting Ranges[a]**

| $k'$ | fitting range for $t'$ | $A$ | $k'_{app}$ | $k'_{D,app} = k'_{app} - k'$ |
|---|---|---|---|---|
| 0.2 | 0−2.5 | 0.96981 | 0.7572 | 0.5572 |
| 0.2 | 0−10 | 0.93797 | 0.6704 | 0.4704 |
| 0.4 | 0−2.5 | 0.98069 | 0.9864 | 0.5864 |
| 0.4 | 0−10 | 0.98069 | 0.9556 | 0.5556 |
| 0.6 | 0−2.5 | 0.98796 | 1.208 | 0.608 |
| 0.6 | 0−10 | 0.98474 | 1.1972 | 0.5972 |
| 1 | 0−2.5 | 0.99624 | 1.636 | 0.636 |
| 1 | 0−10 | 0.99586 | 1.6344 | 0.6344 |
| 2 | 0−2.5 | 1.00392 | 2.67008 | 0.67008 |
| 4 | 0−2.5 | 1.00652 | 4.68692 | 0.68692 |
| 8 | 0−2.5 | 1.00395 | 8.6508 | 0.6508 |
| 20 | 0−2.5 | 1.00075 | 20.5634 | 0.56344 |
| 40 | 0−2.5 | 1.00014 | 40.5268 | 0.5268 |

[a] The dimensionless parameters and variables are defined as $t' = t/(R^2/2D)$, $k' = k/(2D/R^2)$ (where $k$ is the usual pseudo-first-order rate constant), $k'_{app} = k_{app}/(2D/R^2)$, and $k'_{D,app} = k_{D,app}/(2D/R^2)$.

Because the dimensionless diffusion decay constant (the coefficient in eq A9) only weakly depends on the dimensionless decay constant, a fast converging iterative procedure was used. For example (see Table 2), for the middle temperature of 550 K the experimentally measured decay constant is 630 $s^{-1}$, and the estimated $2D/R^2$ is 92 $s^{-1}$. The dimensionless apparent decay constant is $k'_{app} = 630/92 = 6.85$. First, the whole decay constant was assigned to the reaction, $k' \sim k'_{app}$. Interpolation of the last column in Table 3 shows that $k'_{D,app}$ of 0.67 corresponds to this dimensionless decay constant. This value (0.67) was used for all three temperatures as a first guess. Next, a refined value for the decay constant was obtained: $k'_{est} = k'_{app} - 0.67 = 6.85 - 0.67 = 6.18$. A new value for $k'_{D,app}$ that corresponds to $k' = 6.18$ was determined from Table 3. For 550 K, this is still 0.67—the procedure converged in one step. For 522 and 583 K additional steps yielded 0.69 and 0.62 for $k'_{D,app}$, respectively.

## References and Notes

(1) Miller, J. A.; Kee, R. J.; Westbrook, C. K. *Annu. Rev. Phys. Chem.* **1990**, *41*, 345.
(2) Warnatz, J. *Rate Coefficients in the C/H/O System*; Springer-Verlag: New York, 1984.
(3) Tsang, W.; Hampson, R. F. *J. Phys. Chem. Ref. Data* **1986**, *15*, 1087.
(4) Hochgreb, S.; Dryer, F. L. *Combust. Flame* **1992**, *91*, 257.
(5) Eiteneer, B.; Yu, C.-L.; Goldenberg, M.; Frenklach, M. *J. Phys. Chem. A* **1998**, *102*, 5196.
(6) Becerra, R.; Carpenter, I. W.; Walsh, R. *J. Phys. Chem. A* **1997**, *101*, 4185.
(7) Lee, K.-T.; Bowman, J. M. *J. Phys. Chem.* **1986**, *85*, 6225.
(8) Sappey, A. D.; Crosley, D. R. *J. Phys. Chem.* **1990**, *93*, 7601.
(9) Adamson, G. W.; Zhao, X.; Field, R. W. *J. Mol. Spectrosc.* **1993**, *160*, 11.
(10) Neyer, D. W.; Luo, X.; Houston, P. L. *J. Chem. Phys.* **1995**, *102*, 1645.
(11) Tobiason, J. D.; Dunlop, J. R.; Rohlfing, E. A. *J. Chem. Phys.* **1995**, *103*, 1448.
(12) Temps, F.; Stock, C.; Li, X.; Keller, H.-M.; Schinke, R. *J. Chem. Phys.* **1997**, *106*, 5333.
(13) Stumpf, M.; Dobbyn, A. J.; Mordaunt, D. H.; Keller, H. M.; Fluethmann, H.; Schinke, R.; Werner, H. J.; Yamashita, K. *Faraday Discuss.* **1995**, *102*, 193.
(14) Wagner, A. F.; Bowman, J. M. *J. Phys. Chem.* **1987**, *91*, 5314.
(15) Timonen, R. S.; Ratajczak, E.; Gutman, D.; Wagner, A. F. *J. Phys. Chem.* **1987**, *91*, 5325.
(16) De Guertechin, L. O.; Vandooren, J.; Van Tiggelen, P. J. *Bull. Soc. Chim. Belg.* **1983**, *92*, 663.
(17) Browne, W. G.; Porter, R. P.; Verlin, J. D.; Clark, A. H. A Study of Acetylene-Oxygen Flames. *Symp. Int. Combust. Proc.* **1969**.

(18) Pearson, G. S. *J. Phys. Chem.* **1963**, *67*, 1686.
(19) Hidaka, Y.; Taniguchi, T.; Kamesawa, T.; Masaoka, H.; Inami, K.; Kawano, H. *Int. J. Chem. Kinet.* **1993**, *25*, 305.
(20) Bennett, J. E.; Blackmore, D. R. Rates of Gas-Phase Hydrogen-Atom Recombination at Room Temperature in the Presence of Added Gases. *Symp. Int. Combust. Proc.* **1971**.
(21) Hikida, T.; Eyre, J. A.; Dorfman, L. M. *J. Chem. Phys.* **1971**, *54*, 3422.
(22) Ahumada, J. J.; Michael, J. V.; Osborne, D. T. *J. Chem. Phys.* **1972**, *57*, 3736.
(23) Baldwin, R. R.; Jackson, D.; Melvin, A.; Rossiter, B. N. *Int. J. Chem. Kinet.* **1972**, *4*, 277.
(24) Azatyan, V. V.; Andreeva, N. E.; Intezarova, E. I.; Nersesyan, L. A. *Arm. Khim. Zh.* **1973**, *26*, 959.
(25) Wang, H. Y.; Eyre, J. A.; Dorfman, L. M. *J. Chem. Phys.* **1973**, *59*, 5199.
(26) Campbell, I. M.; Handy, B. J. *J. Chem. Soc., Faraday Trans. 1* **1978**, *74*, 316.
(27) Gordon, E. B.; Ivanov, B. I.; Perminov, A. P.; Balalaev, V. E. *Chem. Phys.* **1978**, *35*, 79.
(28) Krasnoperov, L. N., Chesnokov, E. N. Reaction of Unimolecular Dissociation of Formyl Radical, HCO → H + CO, studied over 1−100 Bar Pressure Range. Eastern States Section of the Combustion Institute Technical Meeting, North Carolina State University, Raleigh, NC, 1999.
(29) Krasnoperov, L. N.; Chesnokov, E. N. Unimolecular Dissociation of Formyl (HCO) Radical Studied over 1−100 Bar Pressure Range. 16th International Symposium on Gas Kinetics, Cambridge, U.K., July 23−27 2000.
(30) Krasnoperov, L. N.; Chesnokov, E. N. Unimolecular Dissociation of Formyl (HCO) Radical Studied over 1−100 Bar Pressure Range. 16th International Symposium on Gas Kinetics, Cambridge, U.K., 2000.
(31) Krasnoperov, L. N.; Chesnokov, E. N.; Stark, H.; Ravishankara, A. R. Elementary Reactions of Formyl (HCO) Radical Studied by Laser Photolysis − Transient Absorption Spectroscopy. 17th International Symposium on Gas Kinetics, University of Essen, Essen, Germany, August 24−29, 2002.
(32) Krasnoperov, L. N.; Chesnokov, E. N.; Stark, H.; Ravishankara, A. R. W. Elementary Reactions of Formyl (HCO) Radical Studied by Laser Photolysis − Transient Absorption Spectroscopy. 17th International Symposium on Gas Kinetics, University of Essen, Essen, Germany, 2002.
(33) Krasnoperov, L. N.; Mehta, K. *J. Phys. Chem. A* **1999**, *103*, 8008.
(34) Grebenkin, S. Y.; Krasnoperov, L. N. *J. Phys. Chem. A* **2004**, *108*, 1953.
(35) Mulcahy, M. F. R.; Pethard, M. R. *Aust. J. Chem.* **1963**, *16*, 526.
(36) Horowitz, A.; Calvert, J. G. *J. Phys. Chem.* **1982**, *86*, 3105.
(37) Blacet, F. E.; Loeffler, D. E. *J. Am. Chem. Soc.* **1942**, *64*, 893.
(38) Blacet, F. E.; Heldman, J. D. *J. Am. Chem. Soc.* **1942**, *64*, 889.
(39) Blacet, F. E.; Brinton, R. K. *J. Am. Chem. Soc.* **1950**, *72*, 4715.
(40) Horowitz, A.; Kershner, C. J.; Calvert, J. G. *J. Phys. Chem.* **1982**, *86*, 3094.
(41) Calvert, J. G.; Pitts, J. N. J.; Thompson, D. D. *J. Am. Chem. Soc.* **1956**, *78*, 4239.
(42) Parmenter, C. S.; Albert, W. J.; Noyes, W. A. J. *J. Am. Chem. Soc.* **1963**, *85*, 416.
(43) Kono, T.; Takayanagi, M.; Nishiya, T.; Hanazaki, I. *Chem. Phys. Lett.* **1993**, *201*, 166.
(44) Altmann, J. A.; Doust, T. A. M.; Osborne, A. D. *Chem. Phys. Lett.* **1980**, *69*, 595.
(45) Terentis, A. C.; Stone, M.; Kable, S. H. *J. Phys. Chem.* **1994**, *98*, 10802.
(46) Yadov, J. S.; Goddard, J. D. *J. Chem. Phys.* **1986**, *84*, 2682.
(47) Hochanadel, C. J.; Sworski, T. J.; Ogren, P. J. *J. Phys. Chem.* **1980**, *84*, 231.
(48) Herzberg, G. T. *The Spectra and Structures of Small Free Radicals*; Cornell University Press: Ithaca, NY, 1971.
(49) Van Den Berg, H. E.; Callear, A. B.; Norstrom, R. J. *Chem. Phys. Lett.* **1969**, *4*, 101.
(50) Basco, N.; James, D. G. L.; James, F. C. *Int. J. Chem. Kinet.* **1972**, *4*, 129.
(51) Bass, A. M.; Laufer, A. H. *Int. J. Chem. Kinet.* **1973**, *5*, 1053.
(52) Macpherson, M. T.; Pilling, M. J.; Smith, M. J. C. *J. Phys. Chem.* **1985**, *89*, 2268.
(53) Scherer, J. J.; Rakestraw, D. J. *Chem. Phys. Lett.* **1997**, *265*, 169.
(54) Baggott, J. E.; Frey, H. M.; Lightfoot, P. D.; Walsh, R. *Chem. Phys. Lett.* **1986**, *132*, 225.
(55) Brown, S. S., Ravishankara, A.R. W., Stark, H. *J. Phys. Chem. A* **2000**, *104*, 7044.
(56) Brown, S. S.; Wilson, R. W.; Ravishankara, A. R. *J. Phys. Chem. A* **2000**, *104*, 4976.
(57) Martinez, R. D.; Buitrago, A. A.; Howell, N. W.; Hearn, C. H.; Joens, J. A. *Atmos. Environ. Part A—Gen. Top.* **1992**, *26*, 785.
(58) Chesnokov, E. N.; Krasnoperov, L. N. UV Absorption Spectrum of Formyl Radical, HCO. 5th International Conference on Chemical Kinetics, NIST, Gaithersburg, Maryland, 2001.
(59) Chesnokov, E. N.; Krasnoperov, L. N. Reactions of Formyl Radical, HCO + HCO and HCO + $CH_3$, Studied by Kinetic UV Absorption Spectroscopy. VI Voevodsky Conference on Physics and Chemistry of Elementary Chemical Processes, Academgorodok, Novosibirsk, Russia, July 21−25, 2002.
(60) Mirokhin, Y.; Mallard, G.; Westley, F.; Herron, J.; Frizzell, D.; Hampson, R. NIST Standard Reference Database 17-2Q98 (Chemical Kinetics Database). National Institute of Standards and Technology: Gaithersburg, MD, 1998.
(61) Reid, R. C.; Praustniz, J. M.; Sherwood, T. K. *The Properties of Gases and Liquids*; McGraw-Hill: New York, 1977.
(62) Atkinson, R.; Baulch, D. L.; Cox, R. A.; Hampson, R. F.; Kerr, J. A.; Rossi, M. J.; Troe, J. *J. Phys. Chem. Ref. Data* **1999**, *28*, 191.
(63) Friedrichs, G.; Herbon, J. T.; Davidson, D. F.; Hanson, R. K. *Phys. Chem. Chem. Phys.* **2002**, *4*, 5778.
(64) Krasnoperov, L. N.; Kalinovski, I. J.; Chu, H.-N.; Gutman, D. *J. Phys. Chem.* **1993**, *97*, 11787.
(65) Krasnoperov, L. N.; Niiranen, J. T.; Gutman, D.; Melius, C. F.; Allendorf, M. D. *J. Phys. Chem.* **1995**, *99*, 14347.
(66) Krasnoperov, L. N.; Chesnokov, E. N.; Panfilov, V. N. *Chem. Phys.* **1984**, *89*, 297.